

Metallic nature of strained thin single-crystal $\text{La}_{2/3}\text{Sr}_{1/3}\text{MnO}_3$ films

A. M. Haghiri-Gosnet,^{1,*} M. Koubaa,² A. F. Santander-Syro,^{3,4} R. P. S. M. Lobo,³ Ph. Lecoeur,¹ and B. Mercey⁵

¹*Institut d' Electronique Fondamentale, IEF/CNRS/UMR 8622, Université Paris Sud, Bâtiment 220, 91405 Orsay Cedex, France*

²*Laboratoire de Physique des Matériaux, Faculté des Sciences de Sfax, Boîte Postale 802, Sfax, Tunisia*

³*Laboratoire Photons et Matière, UPR5 CNRS, LPS-ESPCI, Université Pierre et Marie Curie, 10 rue Vauquelin, 75231 Paris, France*

⁴*Laboratoire de Physique des Solides, LPS/UMR 8502, Université Paris Sud, Bâtiment 510, 91405 Orsay, France*

⁵*Laboratoire de Cristallographie et Sciences des Matériaux, CRISMAT,*

6 Boulevard du Maréchal Juin, 14050 Caen Cedex, France

(Received 1 February 2008; published 23 September 2008)

We explore the charge dynamics of a 40-nm-thick strained single-crystal $\text{La}_{2/3}\text{Sr}_{1/3}\text{MnO}_3$ film as a function of temperature. A coherent-incoherent crossover, occurring when the resistivity value approaches the Ioffe-Regel-Mott limit, is observed at $T^* \approx 200$ K in both the dc resistivity and the optical conductivity. This crossover, located far below the metal-insulator transition and the Curie temperature ($T_C = 338$ K), is associated to a rapid decrease in the mobile charge-carrier concentration above T^* . A semiphenomenological model, whose activation energy decreases with the square of magnetization, is used to fit the experimental change of resistivity $\ln \rho / \rho_{\max}$ and thus determine the film metal-insulator (MI) transition that arises 100 K above T^* close to room temperature.

DOI: 10.1103/PhysRevB.78.115118

PACS number(s): 85.75.-d, 75.47.Lx, 78.20.-e

I. INTRODUCTION

Many oxides such as the ferromagnetic manganites¹⁻⁷ apparently violate the Ioffe-Regel-Mott criterion^{8,9} with the absence of resistivity saturation at ρ_{Mott} , in which the mean-free path l becomes comparable with the Fermi wavelength $\lambda_F = 2\pi/k_F$.¹⁰ To reflect this lack of saturation, the term *bad metal* was introduced, meaning a system with a positive resistivity coefficient $\frac{d\rho}{dT} > 0$ above a certain temperature T^* . In the prototypical double-exchange ferromagnet $\text{La}_{2/3}\text{Sr}_{1/3}\text{MnO}_3$ (LSMO), one of the most studied half-metallic manganite, this crossover temperature T^* was suggested to correspond to the dc Mott resistivity ρ_{Mott} .¹¹

In LSMO single crystals¹² and thick films,¹³ the optical conductivity $\sigma(\omega)$ shows a coherent-to-incoherent crossover at T^* , which defines two different metallic phases below T_C (the word incoherent refers to $l < \lambda_F$). At low temperatures in the coherent phase ($T < T^*$), the optical conductivity exhibits a quasi-Drude behavior that can be interpreted using a one-component picture, and is described by an extended Drude formula with a frequency-dependent scattering rate γ^* and optical mass m^* .¹¹ At high temperatures, in the incoherent regime ($T^* < T < T_C$ and $\frac{d\rho}{dT} > 0$), $\sigma(\omega)$ is characterized by a finite-energy peak at around 1 eV that is related to localization. While the crossover temperature T^* is 40 K lower than T_C in single crystals,¹⁴ it has never been measured in a thin strained film.

In this paper, we use optical conductivity to investigate the carrier dynamics of a 40-nm-thick strained LSMO film. We determine the crossover temperature T^* in three independent ways. The charge dynamics is then modeled in a one-component picture with an extended quasi-Drude response. The temperature dependence of the number of carriers is deduced and discussed in the scheme of a coherent-to-incoherent crossover between two metallic phases. Our results show that there is a loss of mobile carriers at high temperature in the incoherent phase, thus providing insight into the charge dynamics of this material.

II. EXPERIMENT

A 40-nm-thick LSMO epitaxial film was deposited on a (001) SrTiO_3 (STO) substrate using a pulsed laser deposition (PLD) method at both reduced substrate temperature (630 °C) and pressure (5×10^{-3} mbar). A two-dimensional (2D) step edge growth mode was observed *in situ* on the streaky reflection high-resolution electron energy diffraction (RHEED) patterns. The detailed description of the sample growth and the procedure to achieve a complete oxygen stoichiometry is reported elsewhere.¹⁵ The out-of-plane lattice parameter was determined from the angular position of the [002] peak in the x-ray diffraction (XRD) pattern, yielding $c = 0.3844$ nm. With an in-plane parameter equal to $a_{\text{STO}} = 0.3905$ nm, the misfit is 0.83%, inducing a tensile strain. The thickness t_{LSMO} was calculated from x , the number of RHEED specular oscillations (two oscillations for one cell and $t_{\text{LSMO}} = \frac{x}{2}c$), and confirmed by a simulation of the XRD spectrum of the LSMO film using a finite-size effect function. The precision on t_{LSMO} is better than 5% in this range ($t \leq 40$ nm) and the surface roughness, deduced from AFM measurements, is about 0.2 nm (half one unit cell). With a thickness smaller than the critical thickness $h_c \approx 47$ nm (Ref. 16) above which the formation of misfit dislocations becomes thermodynamically favorable, our films are fully strained with no extended defects as previously observed using high-resolution electron microscopy (HREM).⁷ Those HREM measurements confirm no significant relaxation of the parameters (constant c/a ratio) from the interface to the surface.

Near-normal-incidence reflectivity spectra were measured from 30 to 8000 cm^{-1} in a Bruker IFS-66V Fourier transform spectrometer using two different combinations of sources, beam splitters and detectors. A Cary-5 grating spectrometer was utilized to record the spectra from 4000 to 30 000 cm^{-1} . The reflectivity was calibrated with a reference Au mirror in the Bruker measurements and with a reference

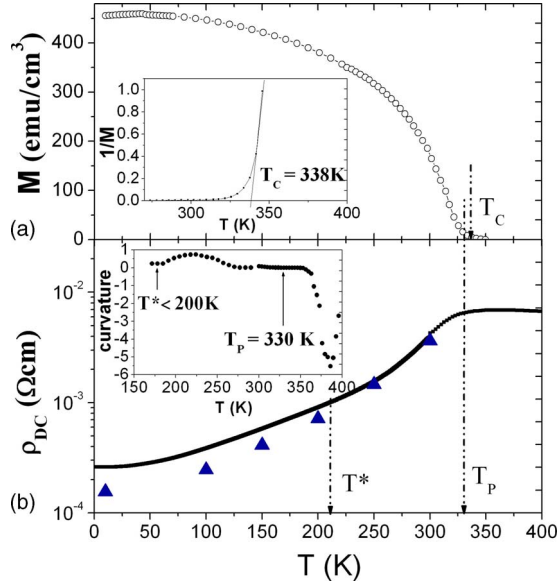


FIG. 1. (Color online) Temperature dependence of (a) the magnetization and (b) the resistivity of the single-crystal LSMO film. The triangles correspond to the $\sigma(\omega \rightarrow 0)$ values deduced from the fits. Inset (a): the Curie-Weiss fit for the determination of T_C . Inset (b): determination of the crossover temperature T^* from the curvature κ (see text).

Ag mirror in the Cary measurements. The spectra were measured, in the whole range, at several temperatures from 10 to 300 K. The agreement of the reflectivity in the overlapping spectral regions for different beam splitters and different spectrometers was better than 1%.

III. RESULTS AND DISCUSSION

The temperature dependence of the magnetization M and the resistivity ρ_{dc} of the single-crystal thin film are presented in Fig. 1. $T_C = 338$ K was determined by extrapolation of the Curie-Weiss law at $1/M = 0$ [see inset of Fig. 1(a)]. We obtain the peak value of ρ_{dc} $T_P = 330$ K, determined from the zero value of the curvature κ [see inset of Fig. 1(b)], where $\kappa = \rho'' / [1 + (\rho')^2]^{3/2}$ and the prime denotes the derivative. As proposed by Bebenin *et al.*,¹⁷ κ can also be used to determine T^* in the temperature range below T_C . As observed in the inset of Fig. 1(b), $\kappa = 0$ at $T \leq 200$ K, which means that T^* is lower than 200 K. Even if manganites violate the Ioffe-Regel-Mott limit,^{8,9} one can estimate the temperature of ρ_{Mott} at which the mean-free path l becomes equal to the interatomic spacing a (i.e., the cell parameter). Assuming a metallic carrier density $n \approx 10^{28} \text{ m}^{-3}$ [with a whole conductance due to the spin majority channel and $N_1(E_F) = 0.58 \text{ states/eV Mn}$ (Ref. 18)] and a Fermi velocity $v_F \approx 7 \times 10^5 \text{ m/s}$,¹⁹ one finds from Drude theory a maximal resistivity,¹⁰

$$\rho_{Mott} \approx \frac{mv_F}{ne^2a} \approx 645 \text{ } \mu\Omega \text{ cm}, \quad (1)$$

and the corresponding Mott conductivity,

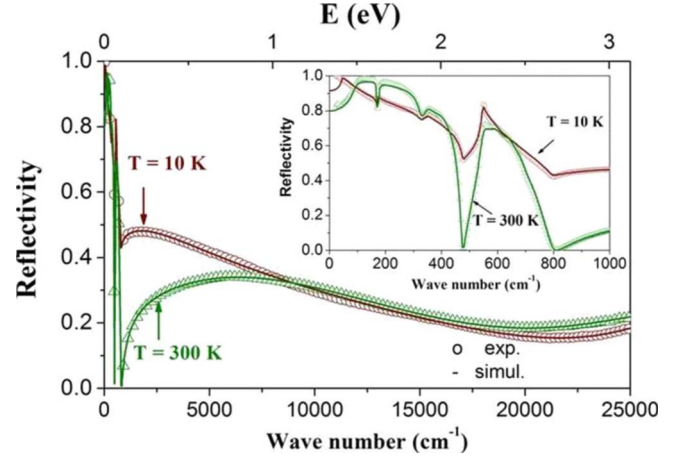


FIG. 2. (Color online) The experimental (circles) and fitted (full line) reflectivity spectra of the LSMO single-crystal film at 10 and 300 K. The low-frequency part of the spectra is shown in the inset.

$$\sigma_{Mott} = 1/\rho_{Mott} \approx 1135 \text{ } \Omega^{-1} \text{ cm}^{-1}. \quad (2)$$

From our dc measurements, $\rho_{dc} = \rho_{Mott} = 645 \text{ } \mu\Omega \text{ cm}$ for the temperature 162 K, which is a first indication of the value of the crossover temperature T^* . At $T > 162$ K, with a mean-free path smaller than the interatomic distance, the film may be considered as a bad metal even if the resistivity exhibits a metallic dependence ($\frac{d\rho}{dT} > 0$). Our dc measurements show the existence of broad coherent-to-incoherent crossover in the range 160–200 K, i.e., ≈ 160 K below T_C at a temperature significantly lower than in a single crystal.¹⁴

Additional insight is gained by considering the optical conductivity. Figure 2 shows the experimental and fitted reflectivity spectra at 10 and 300 K. We fit the experimental spectra using a generalized Drude-Lorentz oscillator model for the dielectric function of LSMO. Simultaneously, we account for the substrate contribution using the optical constants of the substrate, independently measured at each temperature. As discussed in previous research,^{20,21} we use the resulting dielectric function to extract the intrinsic conductivity $\sigma(\omega)$ at each temperature. The resulting real part of the optical conductivity spectra is presented in Fig. 3(b). For comparison with the four-probe dc conductivity data, we extrapolate the conductivity to $\omega = 0$ at each temperature, shown by the triangles in Fig. 1. As described by Takenaka *et al.*,¹¹ the optical method is very sensitive to any surface deterioration. Thus the similar dc and ac conductivity values confirm the high quality of our films. Furthermore this agreement validates our fitting procedure and our determination of $\sigma_1(\omega)$.

At low temperatures, the conductivity spectrum exhibits two components with a dominant coherent Drude-like contribution (a peak centered around $\omega = 0$) and a mid-IR broadband peaking in the range 3000–8000 cm^{-1} . At room temperature, the Drude peak has disappeared and a large mid-IR band dominates at 1 eV, reflecting carrier localization from the interorbital and charge-transfer dominant transitions. In addition to the electrical measurements above, we determined the coherent-to-incoherent crossover temperature T^*

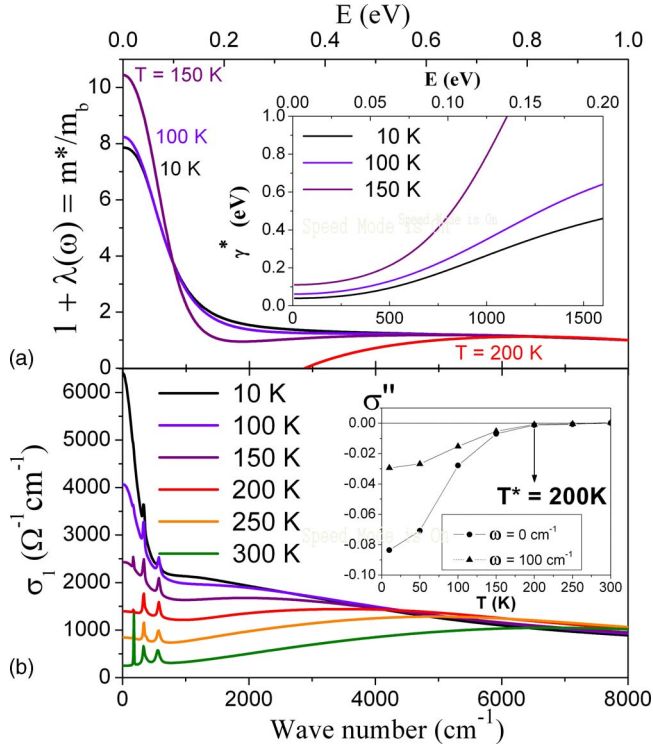


FIG. 3. (Color online) (a) Mass enhancement ratio $\frac{m^*}{m_b}$ (inset: renormalized scattering rate γ^* characteristic of the low ω Drude peak). (b) Real part of the optical conductivity $\sigma_1(\omega)$ of the LSMO film at different temperatures (inset: temperature dependence of σ_1'' for the determination of the crossover temperature T^*). Ω_p required for Eq. (4) has been obtained by setting $\lambda=0$ ($m=m^*$) at 8000 cm^{-1} . Within experimental errors, the same results are obtained for renormalization done at any ω in the $5000\text{--}9000 \text{ cm}^{-1}$ interval.

from the second derivative of the conductivity σ_1'' , as shown in the inset of Fig. 3(b). σ_1'' takes low negative values at low temperatures because of the Drude-like term and vanishes at 200 K, signifying the crossover to the bad-metal phase, consistent with our dc resistivity measurements.

As commonly observed in manganites and other correlated metals, at low temperatures, the observed peak at $\omega=0$ has a quasi-Drude decay. We will show that the use of an extended Drude formalism²² in a one-component picture is well adapted to analyze our data.

The conductivity can be parametrized by a scattering rate,

$$\gamma = \frac{2\pi}{Z_0} \Omega_p^2 \text{Re}\left(\frac{1}{\sigma}\right), \quad (3)$$

where $Z_0=377 \Omega$ is the characteristic impedance of free space, and a mass enhancement ratio,

$$\frac{m^*}{m_b} = 1 + \lambda(\omega) = \frac{2\pi}{Z_0} \frac{1}{\omega} \Omega_p^2 \text{Im}\left(\frac{1}{\sigma}\right). \quad (4)$$

A very useful function in analyzing the low-frequency free-carrier behavior is the screened scattering rate,²³

$$\gamma^* = \frac{\gamma}{1 + \lambda(\omega)} = \omega \frac{\sigma_1}{\sigma_2}. \quad (5)$$

Contrary to γ , the absolute value of γ^* does not depend on the choice for Ω_p^2 and is therefore a more reliable quantity to infer the low ω behavior at the coherent-incoherent phase crossover. Figure 3(a) shows the evolution of $m^*/m_b(\omega)$ and $\gamma^*(\omega)$ of the thin film below 1 eV. The phonon contribution has been subtracted from the fit to highlight the response of the charge carriers. In the coherent phase, at low temperatures, γ^* increases monotonically with ω , as seen in the inset of Fig. 3(a). It shows neither the linear behavior typical of cuprate superconductors nor a ω^2 Fermi-liquid response. At low frequencies, m^*/m_b shows an enhancement that reflects a strong interaction. At larger energies, the carriers are no longer screened and, as expected for a free-electron behavior, m^*/m_b approaches unity. At $T=200 \text{ K}$, the absence of a Drude-like peak makes it impossible to determine m^*/m_b . At the same temperature, γ^* diverges. Thus, above 200 K, the film is in the incoherent phase ($T > T^*$) and the extended Drude formalism can no longer be applied. This is a strong indication that the crossover temperature T^* is slightly lower than 200 K.

A similar approach was used to determine T^* for the single-crystal LSMO with the composition $x=0.4$,¹⁴ where $T^*=310 \text{ K}$ was much closer to T_C . The high-temperature phase in the film appears at a lower temperature $T^* \approx 180 \text{ K}$, which is not surprising since the film has a differently distorted cell due to the internal stress from the STO substrate. However, the conductivity measured at T^* ($\sigma = 1350 \Omega^{-1} \text{ cm}^{-1}$ at $T=180 \text{ K}$) is remarkably close to the one previously reported by Takenaka *et al.* [$\sigma \approx 1600 \Omega^{-1} \text{ cm}^{-1}$ (Ref. 14)] for this single crystal with a different composition.

Using the extended Drude formalism, the renormalized plasma frequency can be expressed as $\Omega_p^{*2} = \Omega_p^2 / [1 + \lambda(0)]$, where $1 + \lambda(0)$ is the dc value of the enhancement factor. Ω_p^2 is the classical plasma frequency, estimated by the integration of the real part of the conductivity $\Omega_p^2 = \frac{Z_0}{\pi^2} \int_0^{\omega_c} \sigma(\omega) d\omega$. Using a cut-off frequency $\omega_c = 8000 \text{ cm}^{-1}$, we estimate a total effective carrier number $N_{\text{eff}} = 0.32$ at 10 K, which is consistent with the doping level $n = 1/3$.

The temperature dependence of the normalized total spectral weight $N_{\text{eff}}/N_{\text{eff-10K}}$, which is proportional to $\Omega_p^{*2}/\Omega_{p-10K}^2$, is reported in Fig. 4 (blue circles). Note that this spectral weight, deduced from the classical plasma frequency, corresponds to the total number of carriers in the film. Its temperature dependence is very similar to that of the magnetization (open circles), which is consistent with theories involving an interplay of double-exchange and electron-phonon couplings.¹³ Moreover, to analyze the carrier dynamics, we also report on the same graph the temperature evolution of $\Omega_p^{*2}/\Omega_{p-10K}^2$. Actually, Ω_p^{*2} reflects only those carriers that participate in coherent transport, and thus $\Omega_p^{*2}/\Omega_{p-10K}^2 = N_{\text{Drude}}/N_{\text{Drude-10K}}$. The number of mobile carriers decays more rapidly with temperature in the 10–200 K range (red diamonds) as a consequence of the strong localization of the carriers.

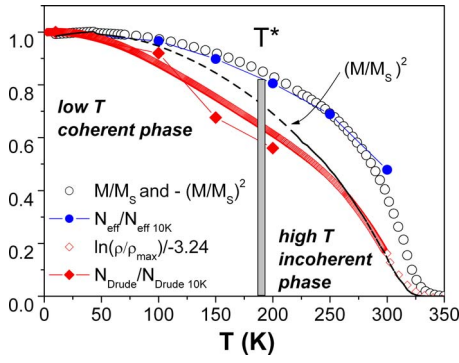


FIG. 4. (Color online) Temperature dependence of both experimental M/M_S (open circle) and $\ln(\rho/\rho_{\max})/-3.24$ (open diamond) in the 40 nm thin strained LSMO film, to be compared with the one of the total number of carriers $N_{\text{eff}}/N_{\text{eff-10K}} = \Omega_p^2/\Omega_{p-10K}^2$ (full circle) and the number of mobile Drude carriers $\Omega_p^{*2}/\Omega_{p-10K}^{*2}$ (full diamond). The $(M/M_S)^2$ curve is also reported (dark line).

To reproduce theoretically the experimental $\rho-T$ curves, Bebenin and Ustinov²⁴ have proposed a simplified semiphenomenological approach based upon physics of disorder in heavily doped semiconductors. An increase in disorder (at $T > T^*$) shifts the mobility edge E_C up to E_F so that the MI transition occurs when $E_C - E_F = 0$. Close to T_C where $(M/M_S) < 0.5$, E_C is assumed to be linear with $(M/M_S)^2$ and the following temperature evolution is expected,

$$\ln \rho/\rho_{\max} = \frac{E_0}{k_B T} - \frac{E_1}{k_B T} (M/M_S)^2, \quad (6)$$

where E_0 and E_1 are constants.

In our investigation, we obtain the experimental relation $\ln \rho/\rho_{\max} = -3.24(M/M_S)^2$. Most notably, $\ln \rho/\rho_{\max}$ has a

similar temperature dependence as $(M/M_S)^2$ for $(M/M_S) < 0.45$ (see open red diamonds and dark line curves in Fig. 4). This validates Bebenin's model in the incoherent metallic phase near T_C . Moreover, the number of mobile carriers $N_{\text{Drude}}/N_{\text{Drude-10K}}$ decays similarly to $\ln \rho/\rho_{\max}$ at low T , which shows that the conductivity of the thin LSMO film can be reliably analyzed using an extended Drude formalism. These temperature dependencies are evidence of an inhomogeneous state near T_C in the tensile strained single-crystal film. Finally from the temperature at which $\ln \rho/\rho_{\max}$ vanishes, we determine the MI transition of the film to be 332 K, close to T_P .

IV. CONCLUSIONS

We find a bad-metal incoherent phase in thin LSMO films that extends over a much larger temperature range (180–330 K) than in the single-crystalline material. The temperature dependence of the number of mobile carriers is shown to decay more rapidly than the total number of carriers in the film. We argue that this loss of metallicity in the temperature range 180–330K is an intrinsic property of the thin film. To clarify the role of stress on the incoherent phase and the crossover temperature T^* , a more extensive investigation of the optical conductivity could be performed on single-crystal LSMO films of varying thickness and strain.

ACKNOWLEDGMENTS

We thank A. J. Millis, M. Bibes, and L. Calvet for helpful discussions. This work has been partially supported by the French network GPB "Matériaux à propriétés remarquables: oxydes supraconducteurs et magnétiques."

*Present address: Laboratoire de Photonique et de Nanostructures, LPN/CNRS/UPR20, route de Nozay, 91460 Marcoussis, France. anne-marie.haghiri-gosnet@lpn.cnrs.fr

¹G. H. Jonker and J. H. van Santen, *Physica (Amsterdam)* **16**, 337 (1950).

²R. M. Kusters, J. Singleton, D. A. Keen, R. McGreevy, and W. Hayes, *Physica B (Amsterdam)* **155**, 362 (1989).

³R. von Helmolt, J. Wecker, B. Holzapfel, L. Schultz, and K. Samwer, *Phys. Rev. Lett.* **71**, 2331 (1993).

⁴K. Chahara, T. Ohno, M. Kasai, and Y. Kosono, *Appl. Phys. Lett.* **63**, 1990 (1993).

⁵S. Jin, T. H. Tiefel, M. McCormack, R. A. Fastnacht, and R. Ramesh, *Science* **264**, 413 (1994).

⁶Y. Tokura and Y. Tomioka, *J. Magn. Magn. Mater.* **200**, 1 (1999).

⁷A.-M. Haghiri-Gosnet and J.-P. Renard, *J. Phys. D* **36**, R127 (2003).

⁸N. F. Mott and E. A. Davis, *Electronic Process in Non-Crystalline Materials* (Oxford University Press, New York, 1979).

⁹A. F. Ioffe and A. R. Regel, *Prog. Semicond.* **4**, 237 (1960).

¹⁰M. Ziese, *Rep. Prog. Phys.* **65**, 143 (2002).

¹¹K. Takenaka, Y. Sawaki, and S. Sugai, *Phys. Rev. B* **60**, 13011 (1999).

¹²Y. Okimoto, T. Katsufuji, T. Ishikawa, T. Arima, and Y. Tokura, *Phys. Rev. B* **55**, 4206 (1997).

¹³M. Quijada, J. Cerne, J. R. Simpson, H. D. Drew, K. H. Ahn, A. J. Millis, R. Shreekala, R. Ramesh, M. Rajeswari, and T. Venkatesan, *Phys. Rev. B* **58**, 16093 (1998).

¹⁴K. Takenaka, R. Shiozaki, and S. Sugai, *Phys. Rev. B* **65**, 184436 (2002).

¹⁵B. Mercey, P. A. Salvador, Ph. Lecoer, W. Prellier, M. Hervieu, Ch. Simon, D. Chippaux, A.-M. Haghiri-Gosnet, and B. Raveau, *J. Appl. Phys.* **94**, 2716 (2003).

¹⁶N. Farag, M. Bobeth, W. Pompe, A. E. Romanov, and J. S. Speck, *Phys. Status Solidi A* **202**, R44 (2005).

¹⁷N. G. Bebenin, R. I. Zainullina, V. V. Mashkautsan, V. V. Ustinov, and Y. M. Mukovskii, *Phys. Rev. B* **69**, 104434 (2004).

¹⁸B. Nadgorny, I. I. Mazin, M. Osofsky, R. J. Soulen, Jr., P. Brousard, R. M. Stroud, D. J. Singh, V. G. Harris, A. Arsenov, and Ya. Mukovskii, *Phys. Rev. B* **63**, 184433 (2001).

¹⁹W. E. Pickett and D. J. Singh, *Phys. Rev. B* **55**, R8642 (1997).

- ²⁰A. F. Santander-Syro, R. P. S. M. Lobo, N. Bontemps, Z. Konstantinovic, Z. Z. Li, and H. Raffy, *Europhys. Lett.* **62**, 568 (2003).
- ²¹A. F. Santander-Syro, R. P. S. M. Lobo, N. Bontemps, W. Lopera, D. Girata, Z. Konstantinovic, Z. Z. Li, and H. Raffy, *Phys. Rev. B* **70**, 134504 (2004).
- ²²B. C. Webb, A. J. Sievers, and T. Mihalisin, *Phys. Rev. Lett.* **57**, 1951 (1986).
- ²³A. El Azrak, R. Nahoum, N. Bontemps, M. Guilloux-Viry, C. Thivet, A. Perrin, S. Labdi, Z. Z. Li, and H. Raffy, *Phys. Rev. B* **49**, 9846 (1994).
- ²⁴N. G. Bebenin and V. V. Ustinov, *J. Phys.: Condens. Matter* **10**, 6301 (1998).